JOC The Journal of Organic Chemistry

Article

pubs.acs.org/joc

Cyclohelminthol X, a Hexa-Substituted Spirocyclopropane from *Helminthosporium velutinum* yone96: Structural Elucidation, Electronic Circular Dichroism Analysis, and Biological Properties

Shizuya Tanaka,[†] Yuna Honmura,[†] Shota Uesugi,[‡] Eri Fukushi,[∥] Kazuaki Tanaka,[†] Hayato Maeda,[†] Ken-ichi Kimura,[‡] Tatsuo Nehira,[§] and Masaru Hashimoto*[,†]

[†]Faculty of Agriculture and Life Science, Hirosaki University, 3-Bunkyo-cho, Hirosaki 036-8561, Japan

[‡]The United Graduate School of Agricultural Sciences, Iwate University, Morioka 020-8550, Japan

[∥]Graduate School of Agriculture, Hokkaido University, Sapporo 060-8589, Japan

[§]Graduate School of Integrated Arts and Sciences, Hiroshima University, 1-7-1, Kagamiyama, Higashi-Hiroshima 739-8521, Japan

Supporting Information

ABSTRACT: *Helminthosporium velutinum* yone96 produces cyclohelminthol X (**1**), a unique hexa-substituted spirocyclopropane. Although its molecular formula and NMR spectral data resemble those of AD0157, being isolated from marine fungus *Paraconiothyrium* sp. HL-78-gCHSP3-B005, our detailed analyses disclosed a totally different structure. Chemical shift calculations and electronic circular dichroism spectral calculations were quite helpful to establish the structure, when those were performed based on density functional theory. The carbon framework of cyclohelminthols I–IV is found at the C1–C8 propenylcyclopentene substructure of **1**. Thus, **1** is assumed to be biosynthesized by cyclopropanation between an oxidized form of cyclohelminthol IV and a succinic anhydride derivative **4**. Cytotoxicity for two cancer cell lines and proteasome inhibition efficiency are measured.

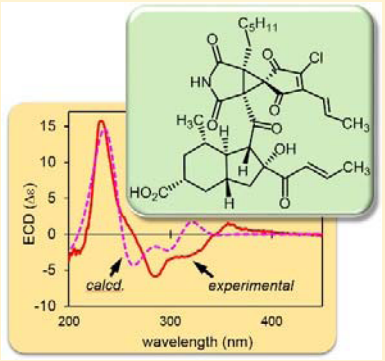

INTRODUCTION

Cyclopropane rings are found in many natural products, such as illudin,[1] coronatine,[2] duocarmycin,[3] ptaquiloside,[4] and curacin A.[5] Their cyclopropane rings play important roles in their biological activities.[6] Additionally, cyclopropane rings have attracted many organic synthetic chemists to establish various effective synthetic methodologies and reactions.[7] We have focused on secondary metabolites from fungi with unique ecologies such as mycoparasites and endophytes to isolate several unique compounds.[8] Recently, we disclosed cyclohelminthols I–IV from *Helminthosporium velutinum* yone96 collected from the dead twigs of a woody plant.[8a] Further investigation of the culture broth resulted in the discovery of cyclohelminthol X (**1**), an unexampled hexa-substituted spirocyclopropane as shown in Figure 1. Although the NMR spectral data of **1** are almost coincident with the data of AD0157 by the group of Quesada,[9] our independent analyses led us to conclude a different structure. Since the core framework of **1** carries only a few protons available for structural elucidation, conventional NMR analyses afforded insufficient structural information. The structure of **1** was established by a combination of density functional theory (DFT) molecular orbital calculations of the NMR chemical shifts as well as the electronic circular dichroism (ECD) spectra. As the core framework of cyclohelminthols I–IV is included in **1**, it enabled us not only to discuss the biosynthesis but also to verify the established structure. The biological properties of **1** are also described.

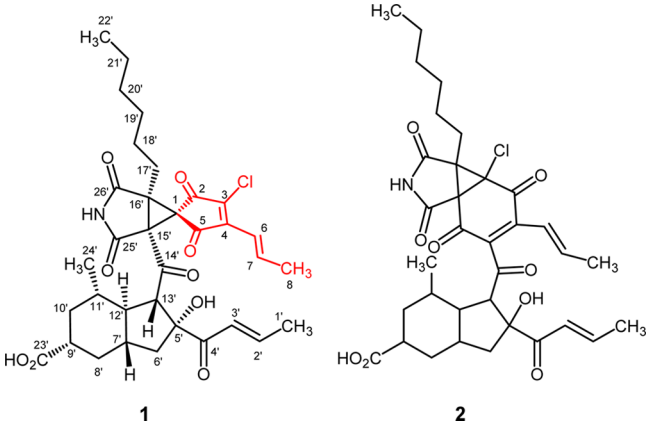

Figure 1. Structures of cyclohelminthol X (**1**) and AD0157 (**2**). The moiety highlighted red is the core framework of cyclohelminthols I–IV.

ISOLATION AND NMR SPECTROSCOPIC ANALYSES

Cyclohelminthol X (**1**) was obtained as an amorphous solid from the culture broth and mycelium of *Helminthosporium velutinum* yone96. This fungus produces cyclohelminthols I–IV which were recently reported by our group.[8a] Cyclohelminthol X (**1**)

Received: February 19, 2017
Published: May 3, 2017

ACS Publications © 2017 American Chemical Society

DOI: 10.1021/acs.joc.7b00393
J. Org. Chem. 2017, 82, 5574–5582

shows a monoisotopic ion at m/z 642.2432 along with the ions due to its isotopologues at m/z 643, 644, 645, and 646 with a 100:38:40:13:2 ratio in the electrospray ionization (ESI) mass spectrum. The signal pattern suggests a chlorine atom in the molecule. Since ESI gives the protonated ion, the even-number mass for the integer part of the monoisotopic ion suggests an odd number of nitrogen(s) in the molecule. The ^{13}C NMR spectrum provides 34 resonances. The HMQC spectrum reveals four methyls, eight methylenes, nine methines, and 13 quaternary carbons, disclosing a total of 37 protons. The ^{1}H NMR spectrum of **1** affords three additional signals at 6.01, 11.47, and 12.04 ppm in DMSO-d_6, which show no HMQC correlation, and these are assigned as protons linked with hetero atoms. These results establish the molecular formula to be $C_{34}H_{40}ClNO_9$ ($[M + H]^+$, calcd m/z 642.2464).

Conventional 2D NMR spectral analyses suggested a 4-carboxy-2-methyl-8-[1-oxo-2-(*E*)-butenyl]bicyclo[4.3.0]-nonane substructure (C1′−C14′ moiety). A literature search was performed based on this planar substructure and to suggest AD0157, being isolated from marine fungus[9] which has the identical molecular formula. The ^{13}C NMR spectral data given in literature matched well with our experimental data in CD_3OD. However, their report mentioned no details about structural elucidation.[9,10] Thus, we had to verify the structure ourselves.

First, the C−Cl linkage was investigated by ^{37}Cl/^{35}Cl-induced ^{13}C isotope shift.[11] We recently demonstrated the effectiveness of this methodology in the structural elucidation of cyclo-helminthols I−IV.[8a] Only the signal at 146.79 ppm splits with a 3:1 ratio, as shown in Figure 2. The chlorine-substituted carbon

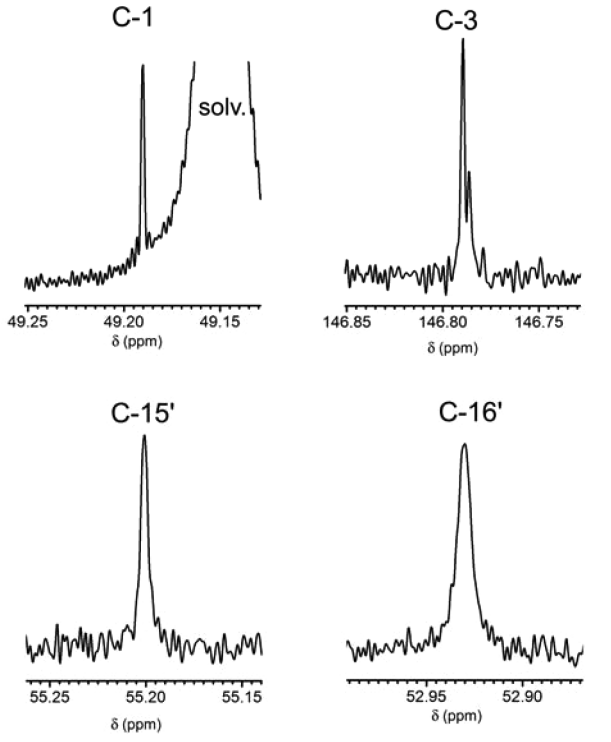

Figure 2. Signal profiles of C-1, C-3, C-15′, and C-16′ resonances in methanol-d_4.

in AD0157 (C18) is assigned as one of the signals at 48.0, 49.7, or 53.9 ppm (the responsible signal has not been specified).[10,12] Thus, the chlorine atom can not be attached to the cyclo-propane moiety as in AD0157 to prove that the present sample is not AD0157. The conclusion is verified by observing similar splitting in the signal at 146.46 ppm in acetone-d_3, while others appear as singlets. These ^{1}H decoupled ^{13}C NMR spectra were taken at high resolution (125 MHz, 128 K data point, zero filling ×4, no broadening factor, no trapezoidal function).

Acetone-d_6 was mainly used as the solvent for further structural elucidation by taking detection of exchangeable protons into account. The data are summarized in Table 1.[13] The *J*-resolved 2D spectrum was helpful in assigning the ^{1}H coupling profiles for some crowded signals. Detailed HMBC spectral analyses disclosed substructures **I** and **II** as shown in Figure 3 (the numbering follows that of the final structure). As the planar structure of substructure **I** (the C1′−C14′ bicyclo[4.3.0]nonane part) has been established, the configuration of substructure **I** was studied next. The H-12′ (1.82 ppm) appears as a double of triplets (J = 10.0 and 11.5 Hz) based on the *J*-resolved 2D spectrum. These large coupling constants suggest that this proton adopts an axial conformation and *anti*-periplanar relationships with H-7′, H-11′, and H-13′. The H-9′ resonance (2.42 ppm) involves two large spin couplings (tt, J = 3.5 and 12.5 Hz), which indicates that this proton adopts an axial configuration. The H-9′ shows ROESY correlation(s) with H-7′ and/or H-11′, which supports the above assignment. The signals for H-7′ and H-11′ are not distinguished in the ROESY spectrum due to signal overlapping. Irradiation of the hydroxyl proton at 3.86 ppm (5′-OH) induces NOEs at Hα-6′ and H-12′. NOEs are also observed at Hβ-6′ and H-13′, when H-3′ is irradiated. These data established a *cis*-relationship between H-13′ and the 1-oxo-(*E*)-2-butenyl side chain.

The other moiety is substructure **II**. Due to its proton-deficient core framework, HMBC was one of the few methods available to obtain the structural information. As described, the C3−Cl linkage has been established. This carbon shows HMBCs with H-6 (6.53 ppm) and H-7 (7.45 ppm). The C-2 and C-5 carbonyls (187.47 and 192.19 ppm, respectively) provide HMBCs with H-6 and H-7, respectively. Additionally, H-6 affords another HMBC signal with C-1 (48.49 ppm). The COSY correlations and the coupling constant between H-6 and H-7 (15.5 Hz) establish the C6−C8 (*E*)-propenyl group. On the other hand, an exchangeable signal at 10.38 ppm affords HMBCs with C-25′ and C-26′ carbonyls (169.14 and 171.42 ppm, respectively) as well as quaternary carbons C-15′ and C-16′ (54.09 and 50.88 ppm, respectively), implying a tetra-substituted succimide substructure. Methylene protons at 2.13 and 2.38 ppm are assigned as α-protons (H_2-17′) of the hexyl side chain, and these protons show HMBCs with C-1, C-16′, and C-26′. Accordingly, the hexyl group should be attached on C16′. Three carbons C1, C15′, and C16′ are assumed to comprise a cyclopropane ring by taking their ^{13}C chemical shifts as well as the unassigned valences into account.

Combining these two substructures would complete the molecule. Substructure **II** requires one more intramolecular bonding for the completion. Candidate structure **A** is obtained by making a linkage between C1 and C2 as well as introducing substructure **I** at C15′. The C17′−C22′ hexyl side chain and substructure **I** should adopt a *cis*-relationship. The *trans*-isomers would involve extraordinary strain because of the 3-azabicyclo[3.1.0]hexane framework, and the succimide ring would readily be cleaved under aqueous conditions. Notably, **1** is stable enough in several solvents at ambient temperature for a couple of days. Since both substructures **I** and **II** are chiral, candidate **A** involves four diastereomers. On the other hand, making a linkage between C2 and C15′ results in candidate **B** after

DOI: 10.1021/acs.joc.7b00393
J. Org. Chem. 2017, 82, 5574−5582

Table 1. Spectral Data of 1 in Acetone-d_6

position	δ^{13}C, type	δ^{1}H, splitting pattern (J in Hz)	HMBC	NOESY
1	48.49, C			
2	187.47, C			
3	146.46, C			
4	149.05, C			
5	192.19, C			
6	120.03, CH	6.53, dq (15.5, 1.6)	1, 2, 3, 4, 7, 8	H_3-8
7	147.93, CH	7.45, dq (15.5, 6.9)	3, 4, 6, 8	H_3-8
8	20.76, CH_3	2.04, dd (1.6, 6.9)	2 (weak), 3, 5, 6, 7	H-6, H-7
1′	18.64, CH_3	1.88, dd (1.6, 6.9)	2′, 3′, 4′	H-2′, H-3′
2′	146.06, CH	6.86, dq (15.4, 6.9)	1′, 3′, 4′	H_3-1′
3′	126.20, CH	6.63, dq (1.6, 15.4)	1′, 2′ (weak), 4′	H_3-1′, Hβ-6′, H-13′
4′	200.63, C			
5′	87.48, C			
6′	45.97, CH_2	: 1.53, dd (11.5, 13.0)	4′, 7′, 8′, 13′	Hβ-6′, 5′-OH
		β: 2.15, dd (6.8, 13.0)	4′, 7′, 12′, 13′	Hα-6′, H-13′
7′	42.98, CH	1.44. ddq (3.0, 8.0, 11.5)	6′, 8′, 11′, 12′	H-9′, (H-13′)
8′	34.43, CH_2	α: 1.22, m	6′, 7′, 9′, 10′, 23′	Hβ-8′, (H-12′)
		β: 2.08, m	9′, 10, 12′, 23′	Hα-8′, H-9′
9′	43.61, CH	2.42, tt (3.5, 12.5)	7′, 8′, 10′, 11′, 23′	H-7′ (and/or H-11′), Hβ-8′, Hβ-10′
10′	39.08, CH_2	α: 1.20, q (12.6)	8′, 11′, 12′, 23′, 24′	Hβ-10′, (H-12′)
		β: 1.94, ddt (1.3, 3.5, 12.5)	8′, 9′, 11′, 12′, 13′, 23′, 24′	H-9′, Hα-10′, H-11″, H_3-24′
11′	37.30, CH	1.48, m	10′, 12′, 24′	H-9′, (H-13′)
12′	53.26, CH	1.82, dd (10.0, 11.5)	6′, 7′, 8′, 10′, 11′, 13′, 14, 24′	Hα-8 (and/or Hα-10), H_3-24′
13′	61.57, CH	4.28, d (11.5)	4′, 5′, 7′, 11′, 12′, 14′	H-3′, Hβ-6′, H-7′ (and/or H-11′)
14′	196.25, C			
15′	54.09, C			
16′	50.88, C			
17′	22.55, CH_2	2.13, NA	1, 15′ (weak), 16′, 18′, 19′, 26′	
		2.38, ddd (4.2, 11.6, 13.7)	1, 16′, 18′, 19′, 26′, 29′	
18′	27.85, CH_2	1.23, m	16′ 19′	
		1.71, m	16′, 17′, 19′, 20′	
19′	30.17, CH_2	1.18, m		
20′	32.17, CH_2	1.27, m		
21′	23.17, CH_2	1.25, m	22′	
22′	14.35, CH_3	0.88, t (6.7)	20′, 21′	
23′	176.50, C			
24′	22.32, CH_3	0.80, d (6.6)	9′, 10′, 11′, 12′	Hα-10′, H-12′
25′	169.14, C			
26′	171.42, C			
5′-OH		3.86	4′, 5′, 6′	Hα-6′
NH		10.38	15′, 16′, 25′, 26′	

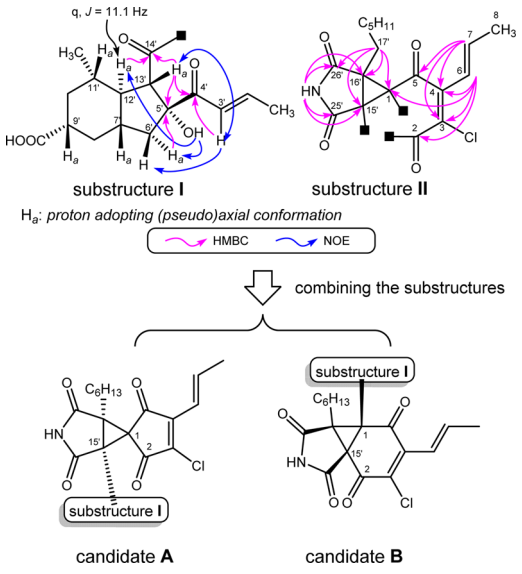

Figure 3. Characteristic HMBC and ROESY correlations on substructures **I** and **II** as well as candidate total structures **A** and **B** obtained by combining these substructures. The substructure **I** was simplified as a box in the candidate structures to emphasize the difference.

introducing substructure **II** at C1. The 9-azatricyclo[6.3.0.0^{1,6}]decane framework causes practically no diastereomers due to the same reason as above.[14] Accordingly, this candidate involves a set of diastereomers. Unfortunately, H-13′ shows no inter-substructural HMBCs despite our trials with several solvents (methanol-d_4, dimethyl sulfoxide-d_6, and benzene-d_6).[15] NOEs were not found between the substructures either. As described, NMR analyses were effective in refining the structure, but not conclusive.

STRUCTURAL DISCUSSION BASED ON THEORETICAL CHEMICAL SHIFTS

Candidate **B** was successfully eliminated by comparing the NMR experimental chemical shifts with those based on DFT molecular orbital calculations.[16] Since the complete structure of **1** involves an enormous number of conformers to be considered, the simplified models shown in Figure 4 were designed; i.e., the C17′−C22′ hexyl group was replaced with a propyl group, and the C9′ carboxy group was removed. Since the C1 spirocarbon is stereogenic in the core part **A**, diastereomeric models **AS** and **AR** were designed. The *S* and *R* refer to the chirality at C1. Model **B** was derived from candidate **B**. Model **Qu**, a model structure for AD0157, was calculated in addition to models **A** and **B**. Since these core parts are chiral, enantiomeric **X**(*S*) and **X**(*R*) were prepared for the X-part in order to cover all diastereomers. A total of eight models were examined in this study, but enantiomers of these models were not considered.

Calculations were performed as a series of (i) conformational search, (ii) structural refinement under conventional conditions, (iii) removal of duplicate conformers, (iv) structural reoptimization considering entropies, (v) calculation of the chemical shifts,

DOI: 10.1021/acs.joc.7b00393
J. Org. Chem. 2017, 82, 5574−5582

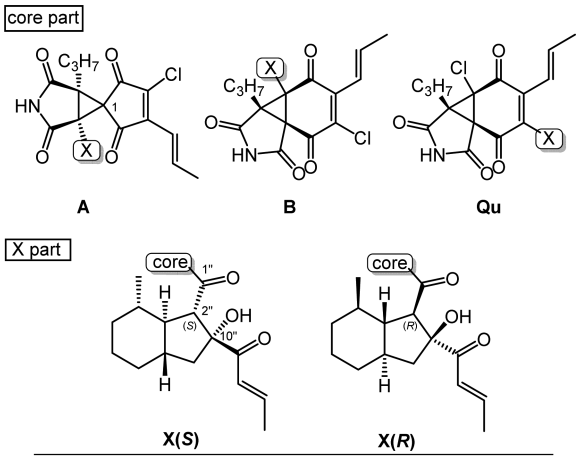

models	core part, (config. at C1)	X part
AS-*S*	A, (*S*)	X(*S*)
AR-*S*	A, (*R*)	X(*S*)
AS-*R*	A, (*S*)	X(*R*)
AR-*R*	A, (*R*)	X(*R*)
B-*S*	B	X(*S*)
B-*R*	B	X(*R*)
Qu-*S*	Qu	X(*S*)
Qu-*R*	Qu	X(*R*)

Figure 4. Models employed for the calculations.

(vi) correction of the chemical shifts with the Boltzmann distribution based on their free energies, and (vii) statistical operations to give the δ_C standard deviations ($\delta_{C_{calcd}} - \delta_{C_{exp.}}$) of the residuals ($\delta_C$ SD, ppm). Conformational searches were performed employing semiempirical AM1, because the searches using molecular mechanism MMFF provided only a limited number of candidate conformers for some models. DFT ωB97X-D[17] was used with 6-31G* basis set for the steps (ii), (iv), and (v). Although entropies (*S*) were not commonly considered, this parameter was added into the calculations by taking the conformational flexibility of the molecules into account.[18] Parameters regarding solvents were not added in these calculations. Stable conformers theoretically distributing more than 90% were subjected to chemical shift calculations. The obtained chemical shifts of 25 carbons were compared with the experimental data in methanol-d_4, acetone-d_6, dimethyl sulfoxide-d_6, chloroform-*d*, and benzene-d_6 to obtain δ_C SD values which serve as scores for comparison. Chemical shifts corresponding to C8′, C9′, C10′, C18′, and C19′ were omitted from the SD estimations because these are close to the removed atoms in the models. The δ_H SD values are less meaningful because of the proton-deficient core frameworks for the **A**, **B**, and **Qu** parts.

The results are summarized in Figure 5. The accuracy level is around 2.0 ppm in this method.[19] These calculations revealed that solvent effects are not critical in all models. Models **B-*S*** and **B-*R*** afford remarkably large δ_C SD values (>4.1 ppm), which enabled us to eliminate them from the candidates. The scores for the AD0157 models **Qu-*S*** and **Qu-*R*** are also not agreeable. In contrast, all diastereomers with the core part **A** provide allowable δ_C SD scores. However, the differences between these scores are not obvious enough to eliminate the others at this stage. Models **AS-*S*** and **AR-*S*** are diastereomers caused by interchanging the C3-chloro and C4-propenyl groups. As shown in Figure 6, these two adopt almost the same stable conformation. The differences between the C3-chloro and C4-propenyl groups hardly affect the δ_C values for 3-azabicyclo[3.1.0]hexane-6-spiro-3-cyclopentene

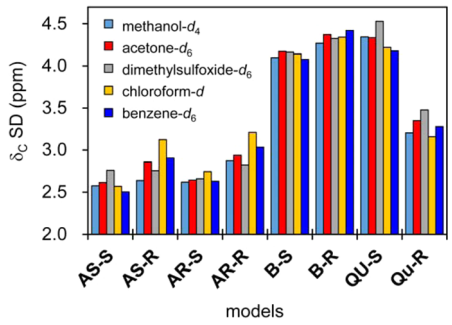

Figure 5. The δ_C standard deviations (δ_C SD, ppm) of the residuals ($\delta_{C_{calcd}} - \delta_{C_{exp.}}$) of model molecules based on ωB97X-D. Experimental data used were those in methanol-d_4, dimethyl sulfoxide-d_6, acetone-d_6, chloroform-*d*, and benzene-d_6.

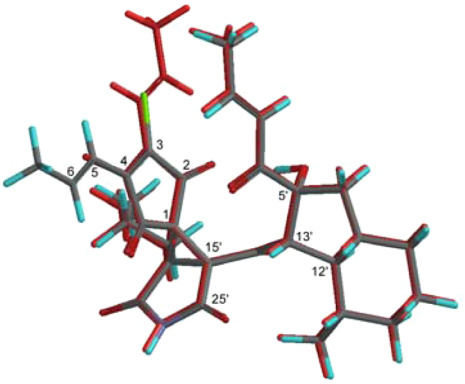

Figure 6. Most stable conformations of model **AS-*S*** (CPK coloring, numbered) and **AR-*S*** (red). The numerals correlate with the numbers of **AS-*S***.

frameworks because of almost symmetrical structures. These differences also hardly affect the carbon chemical shifts on the X-part, since these substructures are spatially apart from the corresponding C3 and C4 to magnetically interact. Similarly, models **AS-*R*** and **AR-*R*** are also diastereomers at C1, and these two models are hardly distinguished in NMR spectroscopic manner. The C1, C15′, and C25′ of the core part and the C5′, C12′, and C13′ of the X part are spatially facing each other. The chemical shift differences are expected to be distinct in these carbons among the diastereomers. When the chemical shift deviations of those chemical shifts from the experimental resonances $\Delta\delta$ [$\delta_{C(benzene)} - \delta_{C(calcd)}$] were compared for these carbons,[20] models **AS-*S*** and **AR-*S*** [(13′*S**,15′*R**)-isomers] afforded significantly smaller deviations than models **AS-*R*** and **AR-*R*** [(13′*R**,15′*R**)-isomers] (Figure 7). The similar

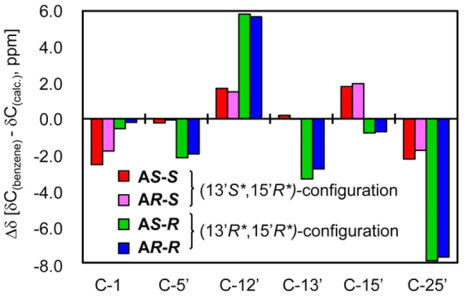

Figure 7. Chemical shift deviations ($\Delta\delta$ [$\delta_{C(benzene)} - \delta_{C(calcd)}$], ppm) of the C-1, C-5′, C-12′, C-13, C-15′, and C-25′ resonances from those of the experimental data in benzene-d_6 for the models **AS-*S***, **AR-*S***, **AS-*R***, and **AR-*R***.

DOI: 10.1021/acs.joc.7b00393
J. Org. Chem. 2017, 82, 5574−5582

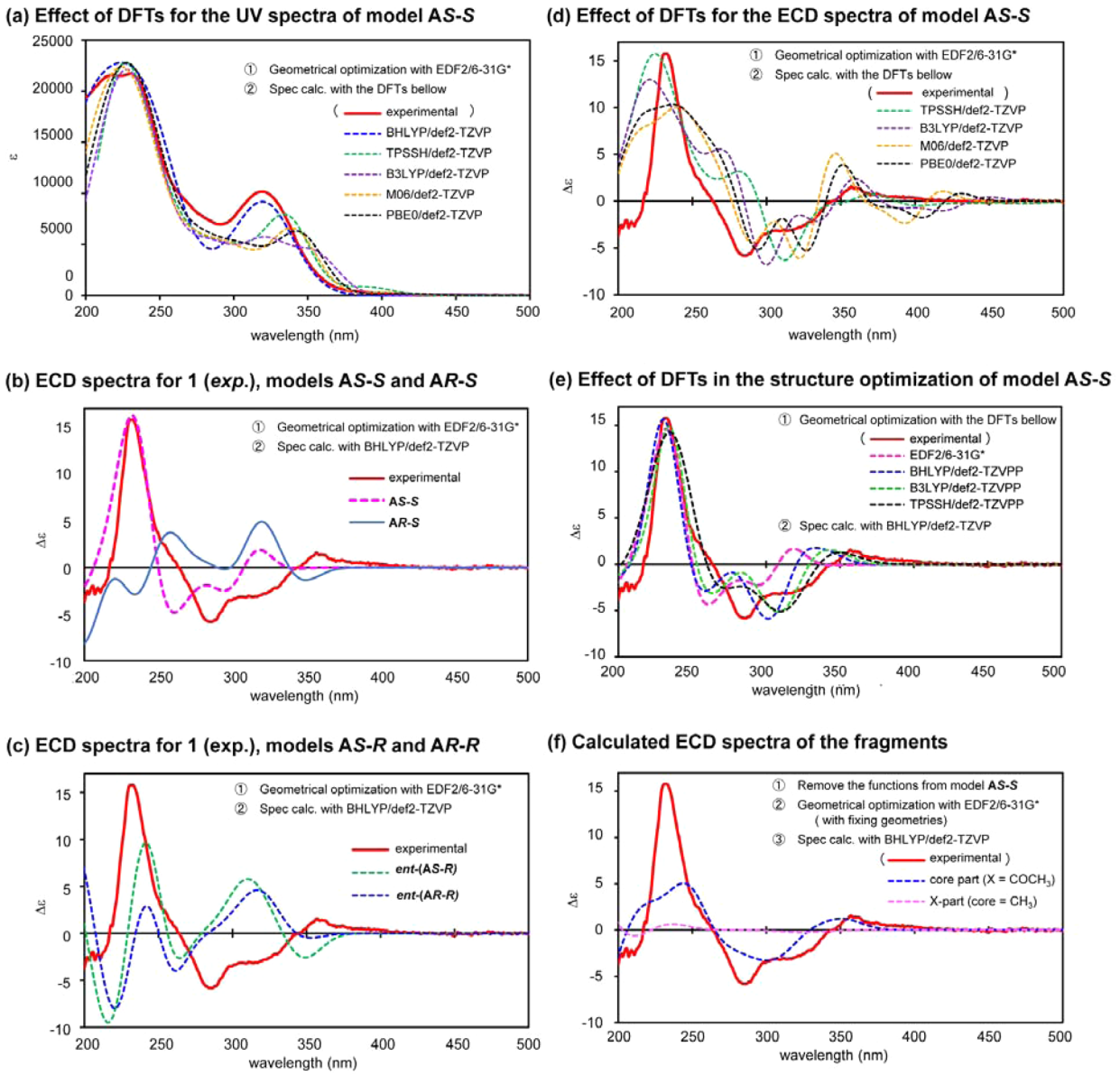

Figure 8. Experimental UV/ECD spectra of **1**, models, and the fragments: (a) theoretical UV spectra of **AS-*S*** with a series of DFTs, (b) theoretical ECD spectra of models **AS-*S*** and **AR-*S*** with BHLYP/def2-TZVP, (c) theoretical ECD spectra of models ***ent*-(AS-*R*)** and ***ent*-(AR-*S*)** with BHLYP/def2-TZVP, (d) theoretical ECD spectra of model **AS-*S*** with a series of DFTs, (e) theoretical ECD spectra of model **AS-*S*** with BHLYP/def2-TZVP after structural reoptimization with a series of DFTs, TPSSH/def2-TZVP, B3LYP/def2-TZVP, M06/def2-TZVP, and PBE0/def2-TZVP, and (f) theoretical independent ECD spectra for the core and X-moieties in model **AS-*S*** with BHLYP/def2-TZVP.

tendency was observed with referring other solvents methanol-d_4, dimethyl sulfoxide-d_6, benzene-d_6, and acetone-d_6 (see Supporting Information). These analyses suggested that isomers with (13′*S**,15′*R**)-configuration (models **AS-*S*** and **AR-*S***) are more plausible than those with (13′*R**,15′*R**)-configuration (models **AS-*R*** and **AR-*R***) as the cyclohelminthol X (**1**). Although model **AS-*S*** afforded the highest score in the chemical shift deviation, chemical shift calculations did not result in conclusive evidence.

■ ECD ANALYSIS WITH THE THEORETICAL SPECTRA

Chiral distortion of chromophores as well as chiral relationships between the chromophores contribute to their ECD. Although models **AS-*S*** and **AR-*S*** adopt almost the same configurations, as shown in Figure 6, these molecules have a distinctly different geometrical relationship between the two chromophores, the C2−C7 dienone and the C2′−C4′ enone. Thus, different profiles are expected in the ECD spectra for models **AS-*S*** and **AR-*S***.

Based on this assumption, ECD spectra of models **AS-*S*** and **AR-*S*** were computed with DFT. Stable conformers theoretically occupying more than 90% cumulative populations based on EDF2/6-31G* (**AS-*S***: 4 conformers, **AR-*S***: 5 conformers) were subjected to the ECD calculations with fixing their geometries. We chose def2-TZVP[21] as the basis set based on our knowledge accumulated in the previous studies.[8a] DFT BHLYP[22] was selected as the functional because of UV spectral reproducibility despite overestimating the energies (requiring wavelength correction +20 nm). Other DFTs (TPSSH,[23] B3LYP,[24] M06,[25] and PBE0[26]) showed considerable discordance in the UV spectra at the $n \rightarrow \pi^*$ region of the chromophores (300−350 nm, R-band), as shown in Figure 8 [spectra (a)]. Fifty excitations

DOI: 10.1021/acs.joc.7b00393
J. Org. Chem. 2017, 82, 5574−5582

were examined in these calculations to express the UV and ECD spectra at 200−500 nm region. The obtained elemental UV and ECD spectra were corrected based on the conformational populations to give the raw spectra. The wavelengths of the raw UV and ECD spectra were uniformly corrected (+20 nm). The ECD intensity for **AS-*S*** was normalized to that of the experimental spectrum at around 235 nm, and the same scale was used for **AR-*S*** to give the ECD spectra [spectra (b)]. Similar computations were performed for models **AS-*R*** and **AR-*R*** to give spectra (c).

As expected, calculations provided totally different ECD spectra for models **AS-*S*** and **AR-*S***. The spectrum for model **AS-*S*** matches very well with the experimental spectrum. On the other hand, no resemblance was found between the theoretical ECD spectrum for model **AR-*S*** and the experimental spectrum. The ECD spectra of model **AS-*S*** were examined with other functionals TPSSH/def2-TZVP, B3LYP/def2-TZVP, M06/def2-TZVP, and PBE0/def2-TZVP in the similar manner as above to obtain agreeable ECD profiles [spectra (d)]. These verified the reliability of the calculated ECD spectra.

However, the theoretical ECD spectrum for model **AS-*S*** in the spectra (b) shows considerable discordance with the experimental ECD at 250−400 nm. The ECD spectrum of this region was found to be quite sensitive for the conformation. When the geometries of model **AS-*S*** were reoptimized with functionals BHLYP, B3LYP, and TPSSH using more accurate def2-TZVPP basis set, the following ECD calculations under the same conditions as above indicated considerable diversity in the ECD profiles at 250−500 nm region, whereas those at 200−250 nm were constant enough [spectra (e)]. Accordingly, we concluded insufficient reproducibility for the ECD profile at 250−350 nm in this model. The UV and ECD at 200−250 nm and 250−400 nm are due to K-band ($\pi \rightarrow \pi^*$ excitation) and R-band ($n \rightarrow \pi^*$ excitation), respectively, of the C2−C7 dienone and the C2′−C4′ enone chromophores.

The individual ECD of these chromophores was estimated for further investigation. The fragment model core-part (X = $COCH_3$ in Figure 4) was prepared by removing atoms of X moiety from the stable conformers of model **AS-*S***-part in the modeling software. The X-part fragment (core = CH_3) was also prepared by removing the core part in a similar manner. These fragments were subjected to ECD calculations (BHLYP/def2-TZVP) by fixing their geometries to give the fragment ECD spectra (f) in Figure 8 after the similar postcomputational operations. The ECDs thus obtained in these calculations are due to chiral torsion of individual chromophores in these fragments. Since only the core part contributes to the ECD at 250−420 nm, the experimental ECDs in this region can be due to R-band ($n \rightarrow \pi^*$ excitation) induced by the chiral torsion of the C2−C7 dienone moiety. It is likely that the chiral torsion of this moiety is so sensitive toward the conformation that static DFT geometrical optimizations can not reproduce the ECDs in that region. On the other hand, the positive Cotton effect at 235 nm is independent of the DFT functionals used in the structural optimizations. All structural optimizations afforded quite similar stable conformations to show a negative chiral relationship between the C2−C7 dienone and the C2′−C4′ enone chromophores, as shown in Figure 9. Since these individual fragments do not show potent ECDs at around 235 nm, the experimental positive ECD in this region can be due to the exciton coupling between the chromophores despite that the negative couplet was not distinctly observed. These chromophores adopt almost parallel relationship in the model **AR-*S***, which may be the reason why this model provided no distinct ECD at around 235 nm.

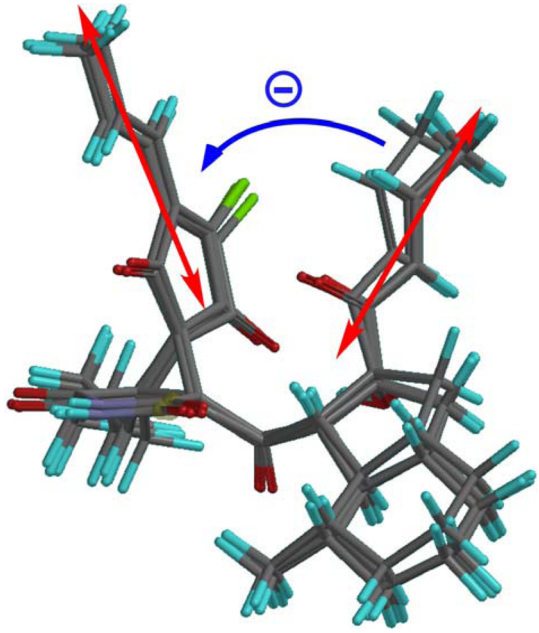

Figure 9. Stable conformations of model **AS-*S*** obtained by optimization with PBE0/def2-TZVPP, BHLYP/def2-TZVPP, B3LYP/TZVPP, and EDF2/6-31G*. The blue arrow is the qualitative definition of the exciton chirality, and the red two-directional arrows are electronic dipole transition moments.

As described, ECD computations revealed that the model **AS-*S*** reproduces the experimental spectrum of **1** the most among all the models. This model has afforded the highest score in terms of δ_C SD values to the experimental NMR spectra. These results allowed us to conclude the overall structure of **1** involving its absolute configuration, as depicted in Figure 1.

BIOSYNTHETIC DISCUSSION

Cyclohelminthol X (**1**) was isolated from the culture broth of *H. velutinum* yone96. The producer fungus also provides cyclohelminthols I–IV.[8a] Interestingly, the framework of these cyclohelminthols is included in **1** (highlighted in red in Figure 1). This suggests that **1** biogenetically belongs to the cyclohelminthol family. Rational biogenesis may become an additional structural support for **1**.

Cyclohelminthol X (**1**) is assumed to be given by cyclopropanation between maleimide **4** and cyclopentadienone **7** *in vivo*, as shown in Scheme 1.[27] The precursor **7** can be derived from cyclohelminthol IV (**5**) by oxidation of the diol to give 2,4-dichloro-1,3-diketone **6** and successive enolization. Since C1 of **7** is nucleophilic, electrophilic maleimide **4** accepts a Michael addition at C16′ to afford C14′−C15′ enol **8**.[28] Regeneration of C14′ ketone would take place in the S_N2-type cyclopropane ring closure to give **1**. Michael addition of **7** at C15′ in **4** can be an alternative pathway. These may proceed enzymatically because no diastereomers were isolated. Although Wessjohann reviewed the biosynthesis of natural cyclopropanes, all cyclopropane frameworks are derived via intramolecular cyclopropanations in that review.[6] Thus, **1** would be the first natural product derived through intermolecular cyclopropanation. Maleimide **4** has not been found from either the broth or the mycelium up to this point. However, the structurally related TAN-1813 is known as a fungal metabolite.[29] Thus, we assume *trans*-decalin **3** as the biosynthetic

DOI: 10.1021/acs.joc.7b00393
J. Org. Chem. 2017, 82, 5574−5582

Scheme 1. Plausible Biosynthesis of 1

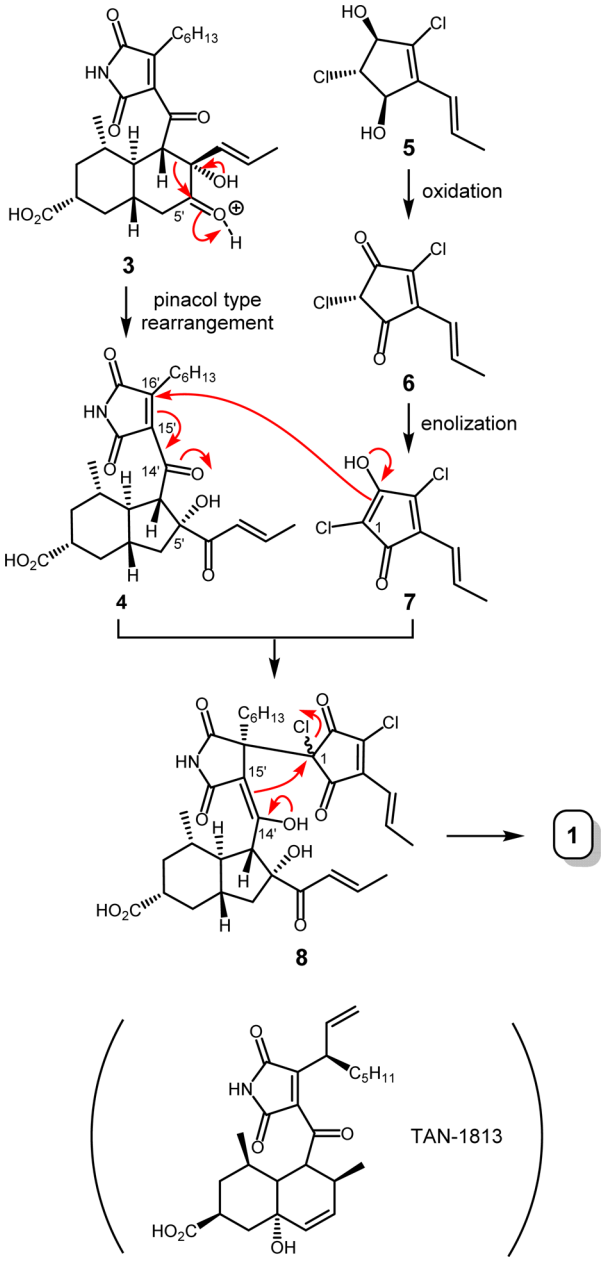

precursor of **4**. Protonation at C5-carbonyl of **3** may induce a pinacol-type ring contraction[30] giving bicyclo[4.3.0]nonane **4**. Oikawa and Tokiwano explained enzymatic intramolecular Diels–Alder cyclization for TAN-1813.[31] They recently proposed the detailed mechanism of enzymatic [4 + 2] cyclization for betaenone, a structurally related *trans*-decalin natural product.[32] The decalin part of **3** can also be derived in a similar manner.

BIOLOGICAL ACTIVITY

The unique structure of **1** led us to be interested in its biological properties. This molecule inhibited the cell growth (IC_{50} 16 μM) of human colon adenocarcinoma cells (COLO 201), and the inhibition effect was more prominent against HL60 human promyelocytic leukemia cells (IC_{50} 0.35 μM) as shown in Table 2. Proteasome inhibitions were also observed against chymotrypsin-like and caspase-like activities (IC_{50} 16.6 and 7.5 μM, respectively) but not against trypsin-like activity (IC_{50} > 50 μM).

Table 2. IC_{50} Values of 1 against COLO201 and HL60 as well as Several Types of Proteasomes

	IC_{50} (μM)
Cytotoxicity	
COLO201 (human colon adenocarcinoma)[a]	16
HL60 (human promyelocytic leukemia)[a]	0.35
Proteasome Inhibition[b]	
chymotrypsin-like	16.6
caspase-like	7.5
trypsin-like	>50

[a]Camptothecin was used as the control (IC_{50} against COLO201:27 μM, HL60:0.02 μM). [b]MG132 was used as the positive control (IC_{50} against chymotrypsin-like: 0.03 μM, caspase-like: 0.6 μM, and trypsin-like; 1.9 μM,).

SUMMARY

We disclosed cyclohelminthol X (**1**) from *H. velutinum* yone96. Although the NMR spectral data of **1** resembled those of AD0157 by Quesada group, the $^{37}Cl/^{35}Cl$-induced ^{13}C isotope-shift analysis enabled us to conclude that **1** is not AD0157. Conventional NMR analyses suggested several candidate structures, which were successfully narrowed down to one structure by theoretical chemical shift calculations and ECD spectral calculations based on DFT. The framework of cyclohelminthols I–IV is included in **1**, which led us to propose a plausible biosynthesis of **1** featuring cyclopropanation between cyclohelminthol IV derivative **7** and maleimide **4**. Cyclohelminthol X (**1**) shows cytotoxicities as well as proteasome inhibitions, although the details remain unknown and are under investigation in our laboratories.

EXPERIMENTAL SECTION

Fungus. *H. velutinum* yone96 was isolated from the dead twigs of a woody plant on Yakushima island, Kagoshima prefecture, Japan in 2007. The fungus was deposited at the Genbank Project, NARO, Japan (ID: MAFF 243859).[33]

Isolation of Cyclohelminthol X (1). *H. velutinum* yone96 was cultured in a potato-dextrose medium, which was prepared from 200 g of potato, 1.0 L of H_2O, and 20 g of glucose. The medium (200 mL) was added into five 500 mL baffled Erlenmeyer flasks, and those were kept on a rotary shaker (110 rpm) at 25 °C for 14 days. The culture medium (20 mL) was dispensed into the freshly prepared potato-dextrose medium (200 mL in each 50 of 500 mL baffled Erlenmeyer flask). The culture thus prepared was stirred on the rotary shaker (110 rpm) at 25 °C for 14 days. The culture broth was filtered, and the filtrate was extracted with EtOAc (ca. 4.0 L). The EtOAc layer was washed with brine, dried over $MgSO_4$, and concentrated *in vacuo* to give the crude extract (2.8 g). After dilution with EtOAc (50 mL), the extracts were dispersed on silica gel (30 g) in a 1.0 L flask, and then the EtOAc was removed with a rotary evaporator. The obtained residue was placed in a silica gel column (400 g) and eluted by 0%, 10%, 15%, 30%, and 50% EtOAc in hexane (1.0 L each). The fraction eluted by 30% EtOAc/hexane was recovered to give a residue (600 mg) after concentration *in vacuo*. The residue was loaded on Sep-Pak ODS (10 g) and eluted with 30%, 50%, 80%, and 100% MeOH in H_2O (200 mL each). The fraction eluted with 100% MeOH was recovered and concentrated *in vacuo*. The residue was subjected to HPLC (SunFire C18, 5 μm, 19 × 150 mm, CH_3CN:H_2O = 65:35, 10 mL/min, detected by UV at 220 nm), which gave cyclohelminthol X (**1**, 16.0 mg) as an amorphous solid; t_R 11.5 min (above conditions). NMR data in acetone-d_6 are given in the main text. The data in dimethyl sulfoxide-d_6, CD_3OD, $CDCl_3$, and benzene-d_6 are also given in the Supporting Information. UV (2.6×10^{-5} mol/L, CH_3CN, ε) 320 nm (10,000), 234 nm (22,000), 217 nm (22,000). ECD (2.6×10^{-5} mol/L, CH_3CN, $\Delta\varepsilon$) 318 nm (−3.0), 285 nm (−5.8), 226 nm (+15). ESIMS *m/z* 642.2432 (100, calcd for $C_{34}H_{41}{}^{35}ClNO_9$, $[M + H]^+$: 642.2470), 644.2422

DOI: 10.1021/acs.joc.7b00393
J. Org. Chem. 2017, 82, 5574–5582

(41, calcd for $C_{34}H_{41}{}^{37}ClNO_9$, $[M + H]^+$: 644.2440), 659.2698, (30, calcd for $C_{34}H_{44}{}^{35}ClN_2O_9$, $[M + NH_4]^+$: 659.2735), 661.2688 (12, calcd for $C_{34}H_{44}{}^{37}ClN_2O_9$, $[M + NH_4]^+$: 661.2706), 664.2256 (19, $C_{34}H_{40}{}^{35}ClNNaO_9$, $[M + Na]^+$: 664.2289), 666.2238 (7.3, $C_{34}H_{40}{}^{37}ClNNaO_9$, $[M + Na]^+$: 664.2260). IR (film) 3260, 2930, 2860, 1785, 1714 (broad), 1630, 1215 cm^{-1}.

Calculations. Conformational searches and chemical shift calculations were performed with Spartan 14 and Spartan 16 (Wavefunction, Irvine, CA) using a PC (operating system: Windows7 Professional; CPU: Intel Xeon E5−1660 v2 processor, 3.70 GHz, 6 cores; RAM: 64 GB). Models were built in the program, and conformational searches were performed with AM1. The search with MMFF afforded only limited numbers of candidate conformers. Suggested stable conformers (15−30 conformers) were optimized successively using HF/321G and ωB97X-D/6-31G*, after duplicate conformers were manually removed and missing conformers were manually added. Suggested conformers were finely refined using EDF2/6-31G* by considering entropy (*S*) using vibrational analysis, and then the chemical shifts of these conformers were calculated using the same approximation. The obtained chemical shifts were corrected using the Boltzmann distribution based on free energies (*G*) to give series of ^{13}C and ^{1}H theoretical chemical shifts, which were analyzed by standard deviations against those of the experimental data.

ECD calculations were carried out with Turbomole 7.0.1 on a workstation (operating system: SUSE Linux Enterprise Desktop 12; CPU: 2× Intel Xeon E5−2687W V4, 3.0 GHz, 12 cores; RAM: 256 GB). Stable conformers occupying more than 90% population based on EDF2/6-31G* were subjected to the ECD calculations (BHLYP/def2-TZVP) with fixing their geometries. Fifty excitations were considered in these calculations. The UV and ECD spectra of each conformer were constructed based on frequencies and rotary strengths using the NORMDIST function in Microsoft Excel 2016. The wavelengths of the spectra were corrected (+20 nm). Theoretical ECD spectra were obtained after correction of the conformational distribution based on the free energy. Similar calculations were performed for models **AS-*S*** and **AR-*S*** with B3LYP,[23] TPSSH,[22] M06,[24] and PBE0[25] using the def2-TZVP basis set. The wavelengths of the UV spectra were corrected to fit the experimental UV spectrum [+20 nm (BHLYP), ±0 nm (TPSSH), +5 nm (B3LYP, M06)]. The intensity of the theoretical ECD spectrum of BHLYP was normalized with that of the experimental spectrum at 235 nm, and the same scale was used for the other ECD spectra. These operations gave the spectra in Figure 8a−d.

The stable conformers of model **AS-*S*** were structurally reoptimized with BHLYP/def2-TZVPP, B3LYP/def2-TZVPP, and TPSSH/def2-TZVPP. The following ECD calculations were performed with BHLYP/def2-TZVP to give the spectra in Figure 8e after postcomputational operations similar to those above.

The X-part moiety was removed from the most stable conformers of model **AS-*S*** on Spartan 16. The obtained fragment structures were subjected to the ECD calculations based on BHLYP/def2-TZVP with fixing their atomic geometries. Similar postcomputational operations afforded the ECD spectrum for the core-part fragment, as shown in Figure 8f. The ECD spectrum for the X-part fragment was calculated in the same manner.

Cytotoxicity Assay against Human Colon Adenocarcinoma COLO 201 Cells. The effect on human colon adenocarcinoma (COLO 201) cell proliferation was measured by WST-1 assay.[34] COLO 201 cells were cultured in RPMI 1640 medium (5×10^3 cells/mL) containing a series of compounds in 96-well tissue culture plates with concentrations of 1.0, 5.0, 10, 50, and 100 μg/mL. After 24 h, 10 μL of WST-1 reagent was added to each well, and the absorbance was measured at 450 nm using a titer-plate reader. Camptothecin was used as the positive control to reveal the IC_{50} (27 μM) by the same protocol.

Cytotoxicity Assay against Human Promyelocytic Leukemia HL60 Cells.[35] Cytotoxicity was measured by MTT assay. HL60 cells (1.0×10^5 cells/ml) were treated with test compounds dissolved in MeOH at the concentrations described above using a 96-well microplate for 2 days. The cells were then incubated for 4 h with 0.5 mg/mL 3-(4,5-dimethylthiazol-2-yl)-2,5-diphenyl tetrazolium bromide (MTT; Dojindo Lab., Kumamoto, Japan). Isopropanol containing 0.04 M aqueous HCl was added to dissolve the MTT formazan reagent product. Percentages of viable cells were calculated as the ratio of the A560 values of treated and control cells (treated with 2% MeOH vehicle for 100 μL of HL60 cells). Camptothecin was used as the positive control to reveal the IC_{50} (0.02 μM) by the same protocol.

***In vitro* Proteasome Assay.**[36] Proteasome activities were measured using a purified human erythrocyte-derived 20S proteasome (Boston Biochem, Cambridge, MA, USA). The fluorogenic compounds, succinyl-L-leucyl-L-leucyl-L-valyl-L-tyrosine 4-methylcoumaryl-7-amide (Suc-LLVY-MCA), *t*-butyloxycarbonyl-L-leucyl-L-arginyl-L-arginine 4-methylcoumaryl-7-amide (Boc-LRR-MCA), and benzyloxycarbonyl-L-leucyl-L-leucyl-L-glutamic acid α-(4-methylcoumaryl-7-amide) (Z-LLE-MCA; Peptide Institute, Inc., Osaka, Japan) were used as substrates for chymotrypsin-like, trypsin-like, and caspase-like activities, respectively. The proteasome (0.05 μg) and test compounds were mixed in assay buffer (pH 8.0, 20 mM Tris-HCl, 0.5 mM EDTA, 0.035% SDS for Suc-LLVY-MCA and Z-LLE-MCA) and preincubated at 30 °C for 10 min. Then, the substrates (50 μM Suc-LLVY-MCA, 20 μM Boc-LRR-MCA, and 20 μM Z-LLE-MCA) were added, and the mixtures were further incubated at 30 °C for 3 h. The fluorescence intensity (excitation/emission wavelength = 360/460 nm) was measured using a Powerscan HT spectrophotometer (Dainippon Sumitomo Pharma, Osaka, Japan). MG132[37] was used as the positive control to reveal the IC_{50} values (against chymotrypsin-like: 0.03 μM, trypsin-like; 1.9 μM, and caspase-like: 0.6 μM) by the same protocol.

■ ASSOCIATED CONTENT

Supporting Information

The Supporting Information is available free of charge on the ACS Publications website at DOI: 10.1021/acs.joc.7b00393.

Copies of ^{1}H NMR, ^{13}C NMR, COSY, HMQC, HMBC spectra of cyclohelminthol X in $CDCl_3$, CD_3OD, acetone-d_6, dimethyl sulfoxide-d_6, and benzene-d_6; summary of the chemical shifts of the models; chemical shift deviations ($\Delta\delta$) of C-1, C-12′, C-13, C-15′, and C-25 resonances from those of the experimental data; stereo structures of the models (PDF)

■ AUTHOR INFORMATION

Corresponding Author

*E-mail: hmasaru@hirosaki-u.ac.jp.

ORCID

Ken-ichi Kimura: 0000-0002-4344-2525

Masaru Hashimoto: 0000-0002-4508-2105

Notes

The authors declare no competing financial interest.

■ ACKNOWLEDGMENTS

We thank Professor Hideaki Oikawa of Hokkaido University for fruitful discussions about the biosynthesis of cyclohelminthol X (**1**). We are also grateful to Dr. Warren J. Hehre of Wavefunction Inc. Part of this work was supported by a Grant-in-Aid for Scientific Research (B) (15H04491) and a Grant-in-Aid for Challenging Exploratory Research (16K14910) from the Japan Society for the Promotion of Science (JSPS). The authors would like to thank Enago (www.enago.jp) for the English language review.

■ REFERENCES

(1) McMorris, T. C.; Anchel, M. *J. Am. Chem. Soc.* **1963**, *85*, 831−832.

(2) Ichihara, A.; Shiraishi, K.; Sato, H.; Sakamura, S.; Nishiyama, K.; Sakai, R.; Furusaki, A.; Matsumoto, T. *J. Am. Chem. Soc.* **1977**, *99*, 636−637.

DOI: 10.1021/acs.joc.7b00393
J. Org. Chem. 2017, 82, 5574−5582

(3) Yasuzawa, T.; Iida, T.; Muroi, K.; Ichimura, M.; Takahashi, K.; Sano, H. *Chem. Pharm. Bull.* **1988**, *36*, 3728−3731.
(4) Niwa, H.; Ojika, M.; Wakamatsu, K.; Yamada, K.; Hirono, I.; Matsushita, K. *Tetrahedron Lett.* **1983**, *24*, 4117−4120.
(5) Gerwick, W. H.; Proteau, P. J.; Nagle, D. G.; Hamel, E.; Blokhin, A.; Slate, D. L. *J. Org. Chem.* **1994**, *59*, 1243−1245.
(6) Wessjohann, L. A.; Brandt, W.; Thiemann, T. *Chem. Rev.* **2003**, *103*, 1625−1648.
(7) (a) Donaldson, W. A. *Tetrahedron* **2001**, *57*, 8589−8627. (b) Chen, D. Y. K.; Pouwer, R. H.; Richard, J.-A. *Chem. Soc. Rev.* **2012**, *41*, 4631−4642. (c) Shoji, M.; Uno, T.; Kakeya, H.; Onose, R.; Isamu, S.; Osada, H.; Hayashi, Y. *J. Org. Chem.* **2005**, *70*, 9905−9915.
(8) (a) Honmura, Y.; Uesugi, S.; Maeda, H.; Tanaka, K.; Nehira, T.; Kimura, K.-i.; Okazaki, M.; Hashimoto, M. *Tetrahedron* **2016**, *72*, 1400−1405. (b) Honmura, Y.; Takekawa, H.; Tanaka, K.; Maeda, H.; Nehira, T.; Hehre, W.; Hashimoto, M. *J. Nat. Prod.* **2015**, *78*, 1505−1510. (c) Takekawa, H.; Tanaka, K.; Fukushi, E.; Nehira, T.; Hashimoto, M. *J. Nat. Prod.* **2013**, *76*, 1047−1051. (d) Murakami, T.; Tsushima, T.; Takada, N.; Tanaka, K.; Nihei, K.; Miura, T.; Hashimoto, M. *Bioorg. Med. Chem.* **2009**, *17*, 492−495. (e) Murakami, T.; Morikawa, Y.; Hashimoto, M.; Okuno, T.; Harada, Y. *Org. Lett.* **2004**, *6*, 157−160.
(9) García-Caballero, M.; Cañedo, L.; Fernández-Medarde, A.; Medina, M. Á.; Quesada, A. R. *Mar. Drugs* **2014**, *12*, 279−299.
(10) Fernández Medrade, A.; Canedo Hernandez, L. M.; Vinuesa Navaro, M. D. L.; Sanchez Lopez, J. M.; Caviro Pelaz, B.; Martinez Insua, M.; Rodrigez Quesada, A.; Garcia Caballeo, M.; Medina Torres, M. Á. WO2015004149 Al, January 15, 2015.
(11) (a) Aliev, A. E.; Harris, K. D. M. *Magn. Reson. Chem.* **1993**, *31*, 54−57. (b) Sergeyev, N. M.; Sandor, P.; Sergeyeva, N. D.; Raynes, W. T. *J. Magn. Reson., Ser. A* **1995**, *115*, 174−182.
(12) All ^{13}C resonances in our experiments appeared at 1.2−1.5 ppm higher frequencies than the corresponding signals of AD0157 in ref 9. We used $^{13}CD_3OD$ signal (49.15 ppm) as internal reference for the δ scale.
(13) Chloroform dissolved **1** poorly to give 1D ^{13}C, HMBC, and HMQC spectra in low quality.
(14) The isomers with *trans*-fused cyclohexenedione ring might theoretically be possible. However, the conjugated system in the cyclohexenedione ring should be chirally twisted in those isomers to induce strong Cotton effects at R-band ($n \rightarrow \pi^*$ excitation, expected to be 300−400 nm), which obviously contradicts the experimental observation that **1** shows very weak CD intensities at that region.
(15) NMR assignments in these solvents were carried out in a similar manner as those in the acetone-d_6, and the data are summarized in Supporting Information.
(16) Di Micco, S.; Chini, M. G.; Riccio, R.; Bifulco, G. *Eur. J. Org. Chem.* **2010**, *2010*, 1411−1434.
(17) Chai, J.-D.; Head-Gordon, M. *Phys. Chem. Chem. Phys.* **2008**, *10*, 6615−6620.
(18) Calculations of entropy require around four times longer time of the calculations than those with default settings.
(19) *Tutorial and User's Guide, Spartan '16 for Windows, Macintosh and Linux*; Wavefunction Inc.: Irvine, CA, 2016.
(20) Since calculations were performed supposing vacuum conditions, the least polar benzene was used as the reference. Carbons are usually hindered by hydrogens. Thus, solvents effect (anisotoropic effect) for ^{13}C chemical shifts is less critical than that for ^{1}H chemical shifts.
(21) Weigend, F.; Ahlrichs, R. *Phys. Chem. Chem. Phys.* **2005**, *7*, 3297−3305.
(22) Becke, A. D. *J. Chem. Phys.* **1993**, *98*, 1372−1377.
(23) Jensen, K. P. *Inorg. Chem.* **2008**, *47*, 10357−10365.
(24) (a) Yanai, T.; Tew, D. P.; Handy, N. C. *Chem. Phys. Lett.* **2004**, *393*, 51−57. (b) Kim, K.; Jordan, K. D. *J. Phys. Chem.* **1994**, *98*, 10089−10094.
(25) Zhao, Y.; Truhlar, D. G. *Theor. Chem. Acc.* **2008**, *120*, 215−241.
(26) Adamo, C.; Barone, V. *J. Chem. Phys.* **1999**, *110*, 6158−6170.
(27) Shimokawa, J.; Harada, T.; Yokoshima, S.; Fukuyama, T. *J. Am. Chem. Soc.* **2011**, *133*, 17634−17637.
(28) Cunha, S.; Rodovalho, W.; Azevedo, N. R.; Mendonça, M. d. O.; Lariucci, C.; Vencato, I. *J. Braz. Chem. Soc.* **2002**, *13*, 629−634.
(29) Ishii, T.; Hayashi, K.; Hida, T.; Yamamoto, Y.; Nozaki, Y. *J. Antibiot.* **2000**, *53*, 765−778.
(30) Snape, T. J. *Chem. Soc. Rev.* **2007**, *36*, 1823−1842.
(31) Oikawa, H.; Tokiwano, T. *Nat. Prod. Rep.* **2004**, *21*, 321−352.
(32) Ugai, T.; Minami, A.; Fujii, R.; Tanaka, M.; Oguri, H.; Gomi, K.; Oikawa, H. *Chem. Commun.* **2015**, *51*, 1878−1881.
(33) *Distribution of Microorganism Genetic Resources*; Genetic Resources Center, NARO: Ibaraki, Japan. http://www.gene.affrc.go.jp/distribution-micro_en.php.
(34) Ishiyama, M.; Shiga, M.; Sasamoto, K.; Mizoguchi, M.; He, P.-G. *Chem. Pharm. Bull.* **1993**, *41*, 1118−1122.
(35) (a) Kimura, K.; Sakamoto, Y.; Fujisawa, N.; Uesugi, S.; Aburai, N.; Kawada, M.; Ohba, S.; Yamori, T.; Tsuchiya, E.; Koshino, H. *Bioorg. Med. Chem.* **2012**, *20*, 3887−3897. (b) Arayama, M.; Uesugi, S.; Tanaka, K.; Maeda, H.; Nehira, T.; Kimura, K.; Hashimoto, M. *Tetrahedron* **2016**, *72*, 1031−1035.
(36) (a) Kusakabe, K.; Honmura, Y.; Uesugi, S.; Tonouchi, A.; Maeda, H.; Kimura, K.; Koshino, H.; Hashimoto, M. *J. Nat. Prod.* **2017**, 10.1021/acs.jnatprod.6b01177. (b) Tsukamoto, S.; Yamanokuchi, R.; Yoshitomi, M.; Sato, K.; Ikeda, T.; Rotinsulu, H.; Mangindaan, R. E.; de Voogd, N. J.; van Soest, R. W.; Yokosawa, H. *Bioorg. Med. Chem. Lett.* **2010**, *20*, 3341−3343. (c) Futamura, Y.; Kawatani, M.; Muroi, M.; Aono, H.; Nogawa, T.; Osada, H. *ChemBioChem* **2013**, *14*, 2456−2463.
(37) Tsubuki, S.; Saito, Y.; Kawashima, S. *Biochem. Biophys. Res. Commun.* **1993**, *196*, 1195−1201.

DOI: 10.1021/acs.joc.7b00393
J. Org. Chem. 2017, 82, 5574−5582